Mössbauer spectroscopy as a tool to predict the catalytic activity of the Fe^{3+} sites in an exchanged Fe/hydroxyapatite system

*J.F. Bengoa[1], S. Campisi[2], A. Gervasini[2], S.G. Marchetti[1]**

1-Centro de Investigación y Desarrollo en Ciencias Aplicadas, Dr. J.J. Ronco (CONICET-CICPBA-UNLP), calle 47N°257. 1900 La Plata, Argentina.

2- Dipartimento di Chimica, Università degli Studi di Milano, via Camillo Golgi 19, 20133 Milano, Italy

J.F. Bengoa ORCID: 0000-0002-0952-8093

S. Campisi ORCID: 0000-0002-5496-7482

A. Gervasini ORCID: 0000-0001-6525-7948

S.G. Marchetti ORCID: 0000-0003-1775-3861

**Corresponding Author: march@quimica.unlp.edu.ar*

Abstract

Catalytic reactions, with iron species as active phase, require specific structural organizations to get good activity and selectivity. Thus, the presence of isolated Fe^{3+} ions or nanoclusters, the capacity to produce Fe^{3+}/Fe^{2+} couples or to chemisorb determined reactive molecules are necessaries in different reactions. Therefore, if the presence of these structural properties could be demonstrated, it could be inferred if the system could be active in determined reaction avoiding the screening of catalytic tests, which represent a hard-work. Mössbauer spectroscopy showed ability to verify that Fe exchanged in hydroxyapatite can produce Fe^{3+}/Fe^{2+} redox couples which give good catalytic performances in the NO_x, N_2O and NH_3 abatement reactions and allowed us to verify that isolated Fe^{3+} sites and Fe_xO_y nanoclusters were able to chemisorb CO molecules. Therefore, it could be speculated that Fe/hydroxyapatite system could be active in catalytic reactions in which the adsorption and dissociation of CO is necessary.

Keywords: catalytic; Mössbauer effect; cluster assembly; Fe; nanostructure

Introduction

Different iron catalytic systems are used in a large number of heterogeneous catalytic processes for the large availability and low cost of iron. Recently, in some environmental processes, in biomass treatment, and in some other primary chemistry reactions, interesting iron-containing catalysts have been developed with success. Among them, it can be mentioned: selective catalytic reduction of NO_x (NH_3-SCR) to harmless N_2 in presence of NH_3 as reducing agent [1] selective catalytic oxidation of NH_3 (NH_3-SCO) [2], Fenton-like heterogeneous reactions with environmental applications [3], hydrocarbon synthesis from syngas (Fischer-Tropsch synthesis) [4].

In order to get active and selective processes, in each of the reactions, Fe-active phase must be present with a specific structural organization to impart suitable properties to the catalysts. Thus, the existence of isolated paramagnetic Fe^{3+} ions or of iron nanoclusters, the capacity to produce Fe^{3+}/Fe^{2+} couples or to chemisorb determined reactive molecules (such as carbon monoxide) are necessaries species or properties in the different reactions. For example, good activity in the NO_x decomposition at low temperature using Fe/zeolites has been related with isolated iron species which would be involved as redox sites in the catalytic cycle [5]. Instead, isolated, dimeric and oligomeric iron species would be responsible for selective catalytic reduction of NO by NH_3, but each of these sites has significant differences in its TOF values [6,7]. Differently, iron catalysts with high activity in selective catalytic oxidation of NH_3 (NH_3-SCO) at low temperature, have a great number of isolated Fe^{3+} sites, which are adequate for ammonia adsorption (Lewis sites) and for generating active oxygen adsorbed species. Conversely, when these catalysts operate at

high temperatures, iron oxide clusters are the predominant active species but the reaction is not selectively directed to N_2, also other N-containing species are formed (in particular N_2O) [8]. Alternatively, liquid-solid advanced oxidation processes (AOPs), for degrading contaminants present in wastewater, require the active presence of Fe^{3+}/Fe^{2+} couples when H_2O_2 is selected as oxidant and iron systems are chosen as catalysts in Fenton-like reactions [9,10]. Finally, in processes such as catalytic CO hydrogenation (Fischer-Tropsch synthesis), other attributes are required to iron catalytic systems. In this reaction, supported nanoclusters of iron species able to chemisorb and dissociate CO molecules, are necessaries [11].

Therefore, if the presence of some of the Fe-species/structures above mentioned in a catalyst is verified, it could be predicted if the solid will be suitable for a targeted reaction. Taking into account these considerations and the excellent capacity of the Mössbauer spectroscopy to characterize materials containing or loading with iron, in the present work, we will study the ability of a selected catalytic system, iron/hydroxyapatite (Fe/HAP), to generate Fe^{3+}/Fe^{2+} couples and to chemisorb carbon monoxide.

Hydroxyapatite (HAP) is a calcium phosphate with an ideal composition of $Ca_{10}(PO_4)_6(OH)_2$ which crystallizes in the hexagonal system. The network is composed of phosphate $[PO_4]^{3-}$ tetrahedra along the *c* axis linking the cations Ca^{2+} between them. These cations are arranged on two non-equivalent sites. Cations on site I (Ca(1)), are ninefold coordinated with oxygens of $[PO_4]^{3-}$ tetrahedra with six shorter bonds that define a trigonal prism and three longer bonds that emerge through the prism faces. While, Ca^{2+} ions on site II (Ca(2)), are sevenfold coordinated with six oxygens belonging to phosphate groups and one hydroxyl group which create an irregular pentagonal pyramid. These calcium ions can be exchanged with monovalent, divalent or trivalent cations [12].

The Fe/HAP system was selected because the authors have worked for some years with it and, in previous works, the interesting catalytic properties in some environmental reactions of air-protection have been shown: selective catalytic reduction of NO by NH_3 (NH_3-SCR), selective catalytic oxidation of NH_3 (NH_3-SCO) and N_2O decomposition [1,13]. Therefore, by selecting one Fe/HAP sample, authors tried to verify experimentally, by Mössbauer spectroscopy, the presence of some of the Fe-species previously mentioned and put them in relation with catalytic activity and properties.

The success of the approach is intended to demonstrate that it is possible to predict whether given iron catalysts will be active or not in targeted reactions with a simpler and quicker approach than realization of screening catalytic tests.

Results

As it was previously mentioned the Fe/HAP sample was thoroughly characterized earlier [1]. Briefly, the determined iron loading was 12.93% wt/wt, the N_2-adsorption/desorption isotherms showed a hysteresis loop typical of mesoporous materials with broad pore

structure and a specific surface area of 82 m^2/g. The XRPD pattern presented, exclusively, the typical reflections of crystalline HAP and any additional iron-containing crystal phases could not be detected. The UV-DRS and Mössbauer spectra allowed to investigate on speciation of iron species. Thus, both isolated Fe^{3+} ions (≈ 85%), replacing the calcium ions in sites (1) and (2) of the HAP, and Fe_xO_y nanoclusters, with a size of about 2-4 nm (≈ 15%), were identified.

The Mössbauer results, obtained working with Fe/HAP after the four treatments mentioned in Methodology section, will be described below.

Cleaning with He

After He cleaning, Mössbauer spectra at 298 and 13 K shown dramatic changes with respect to the as prepared sample (Figures 1 and 2) [1]. Clearly, new peaks with larger isomer shifts (δ) and quadrupole splittings (Δ) have appeared. At room temperature the fitting was performed with three doublets. The first one has the same hyperfine parameters than paramagnetic Fe^{3+} that replace Ca(1) ions (blue line) in the as prepared sample. But its percentage is halved. The other signal (red line assigned to paramagnetic Fe^{3+} replacing Ca(2) ions in the as prepared sample) has disappeared completely. The two new doublets (lines cyan and magenta) have isomer shifts typical of Fe^{2+} ions. Cyan doublet, with larger Δ value, would correspond to Fe^{2+} ions located in less distorted sites corresponding to the replacement of Ca(1). On the other hand, magenta doublet would correspond to Fe^{2+} ions situated instead of Ca(2) (Tables 1 and 2). These assignments will be justified in Discussion section.

These species can be detected at 13 K. But two additional signals, corresponding to relaxing sextuplets, were necessaries to get an adequate fitting. One of these sextuplets (olive signal) has identical hyperfine parameters to that assigned to $Fe_x(III)O_y$ nanoclusters ($2 < \text{size (nm)} < 4$) on the as prepared already studied sample [1]. Instead, the other relaxing sextuplet (wine line) has an isomer shift typical of Fe^{2+} oxides species. With a similar interpretation to already made on this sample, the relaxing sextuplet (wine line) has been attributed to $Fe_x(II)O_y$ nanoclusters. The sum of the percentages of these sextuplets (considering the uncertainty of the fitting) is equal to the starting quantity assigned to $Fe_x(III)O_y$ nanoclusters in the original sample. Other aspect to remark is the presence of a distribution of different neighboring environments to the iron ions. This is evidenced by the widening of the doublets attributed to these sites.

Additionally, the Mössbauer spectrum of the sample at 298 K was obtained after the measurement at 13 K, in order to check that structural changes did not happen as a consequence of the cooling process. As it can be seen in Figure 1 and Table 1, both spectra (before and after cooling) are identical.

In summary, the cleaning of Fe/HAP with a thermal treatment under He flow, has reduced totally the paramagnetic Fe^{3+} ions that replace Ca(2), about 80% of iron ions located in

Ca(1) sites, and about 50% of $Fe_x(III)O_y$ nanoclusters. These values were obtained from the areas of the interactions at 13 K, because at this temperature the differences between the recoil-free fractions of the diverse iron species are minimized.

After CO adsorption, the spectra at 298 and 13 K resemble to that of the as prepared sample. The only difference is the presence of a small shoulder on the side of the high positive velocities. Effectively, the fittings indicate that the principal signals correspond to two doublets with hyperfine parameters nearly identical to that assigned to paramagnetic Fe^{3+} ions that replace Ca(1) and Ca(2) ions. The mentioned shoulder was fitted with two doublets with the same parameters that Fe^{2+} ions that replace Ca(1) and Ca(2) ions, respectively. But now, its percentage is only about 10%. Besides, an important decrease of the diversity of immediate surroundings of the iron, is evidenced by the narrowing of the doublets of these sites. Finally, in the spectrum at low temperature, the relaxing sextuplet assigned to $Fe_x(II)O_y$ nanoclusters have disappeared and the signal of $Fe_x(III)O_y$ nanoclusters have increased its percentage.

Therefore, the CO adsorption on paramagnetic exchanged Fe^{2+} ions and on reduced $Fe_x(II)O_y$ nanoclusters leads to a re-oxidation nearly complete to Fe^{3+} ions and $Fe_x(III)O_y$ nanoclusters.

After verify that there are not blocked magnetically signals at both temperatures, the spectra were measured in a lower range of velocities, with the aim to obtain a better resolution of the peaks (more points for each channel).

Again, it was checked that the cooling treatment in presence of CO atmosphere did not produce structural changes on the sample by measuring a new spectrum at 298 K after the acquisition at 13 K (Figure 1 and Table 1).

Cleaning with dry medicinal air

After the cleaning treatment in dry medicinal air flow, the Mössbauer spectrum at 298 K was identical to that of the as prepared sample (Figure 3 and Table 3). Instead, at 13 K, considerable differences have appeared: both doublets (red and blue lines) showed an important broadening of their lines, evidencing the presence of a wide distribution of different neighboring environments to the two Fe^{3+} populations (Figure 4). Besides, an increasing of the Δ value of the signal corresponding to paramagnetic Fe^{3+} ions that replace calcium in Ca(2) sites was detected, which indicates an increase of the asymmetry of these type of sites (Table 4).

Once again, the absence of structural changes (as consequence of the cooling process) was checked measuring the spectrum at 298 K after the acquisition at 13 K (Figure 3).

After CO adsorption on the sample cleaned with air flow, the only difference detected at 298 K with respect to the as prepared sample is the presence of a very small shoulder on the side of the high positive velocities (Figure 3). Which was fitted with two doublets assigned to Fe^{2+} ions that replace Ca(1) and Ca(2) ions. These changes were more evident in the spectrum at 13 K. The small shoulder was detected again, confirming the reduction of minor percentage of the exchanged Fe^{3+} to Fe^{2+} (about 3%) as a consequence of the CO adsorption. Other relevant difference appeared on Δ value of the doublet corresponding to paramagnetic Fe^{3+} ions that replace calcium in Ca(2) sites. This parameter decreased at the same value of the untreated sample, indicating that the original site symmetry was recovered by CO adsorption (Table 4). Besides, the broad of the distributions of different environments around these exchanged Fe^{3+} ions, decreased in a significant way, as it can be deduced from the narrowing of the doublet lines.

Discussion

Cleaning with He

In the first instance, we will analyze the behavior of Fe/HAP after thermal treatment under He flow, because it can help to understand the exchange mechanism between Fe^{3+} ions and Ca^{2+} of HAP during the preparation step. This process remains unclear yet despite all the specific literature invokes an exchange phenomenon with several metal ions and Ca(I) and Ca(II) ions of HAP. The two more probable explanations mentioned in the literature are:

- a) if the exchange process is performed at low pH, between 2 and 3, the predominant iron species in the solution is $[Fe(H_2O)_5(OH)]^{2+}$ instead of $[Fe(H_2O)_6]^{3+}$. The first Fe species can be exchanged with Ca^{2+} ions without need charge compensation. However, the calcination step (in static air at 773 K) will generate Fe^{3+} cations and the charge balance would be adjusted by the removal of protons of the OH^- groups located at HAP tunnels since, Ca^{2+} ions will not leave the lattice as a consequence of calcination process [14]. The exchange process could be schematized as:

- a1) exchange at pH = 2-3:

$$Ca_{10}(PO_4)_6(OH)_2 + 2[Fe(H_2O)_5(OH)]^{2+} \rightarrow Ca_8[Fe(H_2O)_5(OH)]_2(PO_4)_6(OH)_2 + 2Ca^{2+}_{sol}$$

- a2) calcination in static air at 773 K:

$$Ca_8[Fe(H_2O)_5(OH)]_2(PO_4)_6(OH)_2 \rightarrow Ca_8Fe_2(PO_4)_6O_2 + 12H_2O$$

b) the exchange phenomenon would happen with calcium vacancies production. Therefore, the exchange ratio of Fe/Ca would be of 2/3 [15, 16]. The process could be schematized as:

-b1) exchange:

$Ca_{10}(PO_4)_6(OH)_2 + 2Fe^{3+} \rightarrow Ca_7Fe_2(PO_4)_6(OH)_2 + 3Ca^{2+}_{sol}$

-b 2) calcination in static air at 773 K:

$Ca_7Fe(III)_2(PO_4)_6(OH)_2 \rightarrow Ca_7Fe(III)_2(PO_4)_6O + H_2O$

When the preparation steps have concluded, the sample was heated under He flow at 773 K. Mössbauer spectra after this treatment clearly showed a partial iron ions reduction ($Fe^{3+} \rightarrow Fe^{2+}$). We assume that, the thermal treatment with an inert stream in the absence of oxygen, could produce oxygen vacancies in the HAP lattice. As a consequence, in order to maintain the crystal electroneutrality, an auto-reduction of a fraction of Fe^{3+} ions should take place. This process would be more feasible if the solid composition is $Ca_8Fe_2(PO_4)_6O_2$ instead of $Ca_7Fe(III)_2(PO_4)_6O$, because more labile oxide ions would be available in the first case (note that oxygen atoms belonging to phosphate ions have less mobility). This auto-reduction in He flow at 773 K could be schematized as:

$Ca_8Fe(III)_2(PO_4)_6O_2 \longrightarrow Ca_8Fe(III)_{2-2x}Fe(II)_{2x}(PO_4)_6O_{2-x} + ½\ xO_2$

Similar results have been detected in zeolites exchanged with Fe^{3+} [17, 18].

From this analysis we propose that the Ca^{2+} ions exchanged by Fe^{3+} ions in HAP solid, would occurs without production of calcium vacancies.

After the fitting of the Mössbauer spectra of Fe/HAP, treated with He stream at 773 K, is necessary to assign the Fe^{2+} doublets to the different Ca sites. For it, must be considered that, in Fe^{2+} in high spin state, the six 3d-electrons dominate the magnitude of the electric field gradient (V_{zz}^{val}), although in a way that can be determined by the lattice symmetry (V_{zz}^{lat}). Thus, it has been demonstrated by theoretical and experimental results, that if a Fe^{2+} ion in high spin state is located in an environment with an increasing asymmetry, the quadrupole splitting decreases [19-22]. When an Fe^{2+} ion has an environment with perfect cubic symmetry, little or no quadrupole splitting is observed. In this situation, $V_{zz}^{val} = V_{zz}^{lat} = 0$. But, if this symmetry is slightly distorted, in general a very large splitting of about 3.70 mm/s, is observed, almost entirely due to V_{zz}^{val}. As the environment distortion is increased, V_{zz}^{lat} increases and, since it has opposite sign to V_{zz}^{val}, a decreasing of the quadrupole splitting is observed. It is a reverse situation to that of the high spin Fe^{3+} ions, in which the five 3d electrons occupy one atomic d-orbital each and form a half-closed shell. This arrangement has spherical symmetry and does not contribute to an electric field gradient. In this case the quadrupole splitting measures directly the lattice symmetry around the atom. Taking into account these considerations, the Fe^{2+} doublet with higher Δ was assigned to iron ions replacing calcium in sites Ca(1), which are more symmetric and have produced a doublet with the lower Δ for Fe^{3+} ions.

The proposition about the Fe^{3+} auto-reduction by oxygen vacancies production would be in accordance with the complete reduction of Fe^{3+} located in sites Ca(2), which are

coordinated to OH^- groups, because these oxygen atoms appear as more labile than that are coordinated in PO_4^{3-} tetrahedrons.

The detection of a small relaxing sextuplet, with isomer shift typical of Fe^{2+}, would indicate that the oxygen vacancies production, on the surface of $Fe(III)_xO_y$ nanoclusters, have occurred as a consequence of the calcination in He flow, appearing $Fe(II)_xO_y$ nanoclusters. This effect has been frequently observed in nanocrystals of iron oxides heated under inert flow [23].

When cleaned and activated Fe/HAP surface is contacted with CO, the spectra at both temperatures (298 K and 13 K) are nearly identical to that of the as prepared sample. The only detected difference is a small shoulder, as it was previously described, which was fitted using two doublets with the same hyperfine parameters of the Fe^{2+} species. These signals represent only a small percentage (about 10%). This little but important change of the recorded spectra indicates that there is a strong interaction between Fe^{2+} ions, located at both Ca^{2+} exchanged sites, and CO molecules. As consequence, a charge density transfer can occur from Fe^{2+} to adsorbed CO molecules. This effect is clearly reflected by the important change of isomer shifts of both doublets from about 1.2 mm/s (typical value of Fe^{2+} ions) to about 0.5 mm/s (typical value of Fe^{3+} ions) at 13 K. This is an unexpected result because it is well known that CO is a nucleophilic molecule. Therefore, a predictable result would be a reduction of Fe^{3+} ions by CO adsorption as it was found by Kefirov et al. in Fe-BEA zeolite system [24]. We can model this behavior considering that the environment of the lattice sites with oxygen vacancies have a deficiency of local negative charge. The CO molecules, adsorbed on Fe^{2+} ions, would experience a strong electrostatic field due to this lattice charge deficiency, which would produce a polarization of molecule charge. In this situation, Fe^{2+} ions can donate *d* electrons density to π^* antibonding orbitals of CO molecules. As consequence of this process, Mössbauer spectroscopy detect a decreasing of *d* electron population on Fe ions. The low percentage of remaining Fe^{2+} ions would be located in sites that would be inaccessible to CO molecules.

The CO adsorption would complete the coordination sphere of iron ions in both exchangeable sites and the Δ values resemble with the original sample.

Up to our knowledge, this is the first report studying CO adsorption on Fe exchanged with HAP using Mössbauer spectroscopy.

Cleaning with dry medicinal air

The Mössbauer spectrum at room temperature, after thermal treatment in air flow, is identical to that of the as prepared sample. As it was expected, no Fe^{2+} species were detected. At 13 K only Fe^{3+} species were detected too, but the shape of the spectrum looks very different to that the as prepared sample. However, the number of interactions and their hyperfine parameters, obtained from the fitting, are nearly identical to that of the as prepared sample, the only detected change is an increase in the Δ value of Fe^{3+} located

in Ca(2) sites. The original spectrum was obtained using the sample stored under ambient conditions without any previous treatment. Therefore, the solid was hydrated and water molecules could complete the coordination spheres of Fe^{3+} ions in both exchangeable sites leading to a more symmetric environment. After cleaning step, water molecules were eliminated and the surrounding of Fe^{3+} ions become more asymmetric, especially in Ca(2) sites. Under air flow HAP lose water up to 773 K [25]. Therefore, a broad distribution of different iron environments with distinct number of coordination water molecules could be present. This is reflected by the important widening of the lines of both doublets, changing the aspect of the spectrum at 13 K.

All these effects disappeared after CO adsorption, showing that CO species can be adsorbed on both types of Fe^{3+} sites. As it was mentioned previously, there are not studies about the CO adsorption behavior on Fe/HAP system. For this reason, we compare our results with previous reports in systems of zeolites exchanged with iron in which CO was adsorbed. From these references, there is a widespread opinion that Fe^{3+} sites are coordinatively saturated in these systems and they are not able to interact with this probe molecule [26]. Therefore, we can conclude that both Fe^{3+} sites in HAP system are coordinatively unsaturated.

Besides, a small shoulder appears on high velocities side, which was fitted with two doublets with the same hyperfine parameters of Fe^{2+} species previously described. It must be remarked that these sites are different from those that remains without oxidize on Fe/HAP cleaned with He and contacted with CO because, these sites would not be accessible to this probe molecule. Instead, the Fe^{2+} sites, in Fe/HAP cleaned with air and contacted with CO, were reduced by this probe molecule, therefore are accessible to this species. The percentage of these sites is lower than that the inaccessible sites ($\cong$ 3% vs. $\cong$ 10 %, respectively). The reduction of Fe^{3+} exchanged by CO has been previously reported in Fe/zeolite systems [24].

Conclusions

The results of the present work have shown the ability of Mössbauer spectroscopy to verify that Fe exchanged ions in HAP can produce Fe^{3+}/Fe^{2+} redox couples depending on atmospheres and thermal conditions. This is a relevant result to decide the use of Fe/HAP in determined catalytic applications. The good catalytic performances in the NO_x, N_2O and NH_3 abatement reactions of this composite allowed us verify this conclusion [1].

On the other hand, the isolated iron sites and the Fe_xO_y nanoclusters were able to chemisorb CO molecules. Therefore, it could be speculated that the system Fe/HAP could be active in catalytic reaction in which the adsorption and dissociation of this molecule is necessary. Catalytic tests should be done in order to verify this conclusion. But, considering that iron sites could donate *d* electrons density to π^* antibonding orbitals of CO molecules, a weakening of C-O bond could be possible. This effect is necessary to produce a CO dissociation. Only a low percentage of these sites (about 10%) are not

suitable to chemisorb CO. We attribute this result to their location in inaccessible sites to molecules with kinetic diameters higher than 0.38 nm (kinetic diameter of CO molecule).

Finally, from the present results strong evidence that, during preparation steps of Fe/HAP, iron ions would be exchanged with calcium ions without production of calcium vacancies, was obtained.

Methodology

Materials and Catalyst Preparation

Hydroxyapatite (HAP) used in this work was kindly supplied by Soda Ash & Derivatives (Solvay, Brussels, Belgium). Its preparation procedure, composition and main properties were reported in a previous work [27].

An iron functionalized hydroxyapatite sample, with 13% (wt/wt) of iron loading, was prepared using $Fe(NO_3)_3.9H_2O$ (from Sigma Aldrich Chemie GmbH, Germany) by a modified ion exchange (IE) method, called *flash ionic exchange* due to the short contact time of HAP in the Fe-solution [13]. A solution of 250 cm^3 of $Fe(NO_3)_3.9H_2O$ (0.06 M) was thermostated at 313 K. The pH of this solution was adjusted to about 3 by HNO_3 addition to prevent the hydrolytic polymerisation of iron(III). Approximately 6 g of HAP powder, previously dried at 393 K overnight, were added to the iron(III) solution and the obtained suspension was vigorously stirred at 313 K for 15 min. This short contact time assured to preserve both surface and structural properties of HAP, which are sensitive to amorphization or dissolution in an extremely acidic environment [28]. The sample, named Fe/HAP, was filtered, thoroughly washed, dried at 393 K overnight and finally calcined at 773 K for 1 h under static air at controlled rate (1 K/min).

With the aim to study the ability of Fe/HAP system to generate Fe^{3+}/Fe^{2+} couples and to chemisorb CO, the following assays were performed in a home-made cell specially designed and built for the purpose [29]:

-1) the sample was calcined at 773 K for 1 h under He flow (Q_{He}= 60 cm^3/min) at controlled rate (1K/min). Then, was cooled under He flow, the cell was closed and the Mössbauer spectra were measured at 298, 13 and again at 298 K in He atmosphere.

-2) the sample was calcined in the same conditions than **1)**. When room temperature was reached, He flow was replaced by a CO stream (80 cm^3/min) during 4 ½ h. This time was enough in order to sweep the He and to get the CO adsorption on the cleaned sample surface. Finally, the cell was closed and the Mössbauer spectra were measured at 298 and 13 K in CO atmosphere.

-3) the sample was calcined in the same conditions than **1)** but using dry medicinal air flow (Q_{air}= 60 cm^3/min) instead of He. Then, it was cooled under air flow, the cell was closed and the Mössbauer spectra were measured at 298, 13 and 298 K in air atmosphere.

-4) the sample was calcined in the same conditions than **3)**. When room temperature was reached, air flow was replaced by a CO stream (80 cm^3/min) during 4 ½ h. This time was enough in order to sweep the air and to get the CO adsorption on the cleaned sample surface. Finally, the cell was closed and the Mössbauer spectra were measured at 298 and 13 K in CO atmosphere.

The mentioned cell allows us to perform different thermal treatments in distinct atmospheres and to measure the Mössbauer spectra in the same atmosphere avoiding the contact of the sample with air.

Characterization

HAP and Fe/HAP were characterized by atomic absorption spectroscopy (AAS), N_2 adsorption–desorption isotherms at 77 K, X-ray Powder Diffraction (XRPD), UV Diffuse Reflectance Spectroscopy (UV-DRS) and Mössbauer Spectroscopy. These results were previously reported in [1], therefore, in this section, only the characteristics of Mössbauer spectroscopy technique will be described.

Mössbauer Spectroscopy

Mössbauer spectra were obtained in transmission geometry using a 512-channel constant acceleration spectrometer (WissEl, Starnberg, Germany), provided with a source of ^{57}Co in Rh matrix of nominally 50 mCi. The ideal thickness of the sample was evaluated considering the weight percentages of the different elements of each catalyst (ca. 100 mg of powder was used in a holder with diameter of ca. 1.8 cm). The reference used for the velocity calibration was a 12-μm-thick α-Fe foil. Spectra were collected at 13 and 298 K. Measurements at low temperatures were performed working with a closed-cycle cryogenic system (Model DE-202, ARS, Macungie, PA, USA). Each spectrum was folded to minimize geometric effects. The experimental data were fitted using Recoil [30], a commercial program with constraints.

Acknowledgements

The authors acknowledge the financial support of FONCyT-ANPCyT (PICT 2017-2808), CONICET and CICPBA which allowed the development of this work.

Declarations

Funding: ANPCyT (PICT 2017-2808).

Conflicts of interest/Competing interests: On behalf of all authors, the corresponding author states that there is no conflict of interest.

Availability of data and material: All data generated or analyzed during this study are included in this published article.

Code availability: Not applicable.

Authors' contributions: These authors contributed equally to the work

References

[1] M.G. Galloni, S. Campisi, S.G. Marchetti, A. Gervasini, Catalysts, 10, 1415(2020). Catalysts 2020, 10, 1415; https://doi.org/10.3390/catal10121415.

[2] S. Campisi, S. Palliggiano, A. Gervasini, C. Evangelisti,, J. Phys. Chem. C, 123 11723 (2019). https://doi.org/10.1021/acs.jpcc.9b01474.

[3] S. Giannakis, Appl. Catal. B: Environ. 248, 309 (2019). https://doi.org/10.1016/j.apcatb.2019.02.025.

[4] I.O. Pérez De Berti, J.F. Bengoa, S.J. Stewart, M.V. Cagnoli, G. Pecchi, S.G. Marchetti, J. Catal. 335, 36 (2016). https://doi.org/10.1016/j.jcat.2015.12.004.

[5] R. Zhang, N. Liu, Z. Lei, B Chen, Chem. Rev., 116, 3658 (2016). https://doi.org/10.1021/acs.chemrev.5b00474.

[6] O. Kröcher, S. Brandenberger, Chimia, 66, 687 (2012). https://doi:10.2533/chimia.2012.687.

[7] S. Brandenberger, O. Kröcher, A. Tissler, R. Althoff, Appl. Catal. B: Environ., 95, 348 (2010). https://doi.org/10.1016/j.apcatb.2010.01.013.

[8] R. Q. Long, R. T. Yang, J. Catal., 207, 158 (2002). https://doi.org/10.1006/jcat.2002.3545.

[9] N. Thomas, D.D. Dionysiou, S.C. Pillai, J. Hazard. Mater. 404, 124082 (2021). https://doi.org/10.1016/j.jhazmat.2020.124082.

[10] S.S. Lin, M.D. Gurol, Environ. Sci. Technol., 32, 1417 (1998). https://doi.org/10.1021/es970648k.

[11] L.A. Cano, M.V. Cagnoli, J.F. Bengoa, A.M. Alvarez, S.G. Marchetti S.G., J. Catal. 278, 310 (2011). https://doi.org/10.1016/j.jcat.2010.12.017.

[12] A. Fihri, Ch. Len, R.S. Varma, A. Solhy, Coordination Chem. Rev., 347, 48 (2017). https://doi.org/10.1016/j.ccr.2017.06.009.

[13] S. Campisi, M.G. Galloni, S.G. Marchetti, A. Auroux, G. Postole, A. Gervasini, ChemCatChem, 12, 1676 (2020). https://doi.org/10.1002/cctc.201901813.

[14] M. Khachani, M. Kacimi, A. Ensuque, J-Y. Piquemal, C. Connan, F. Bozon-Verduraz, M. Ziyad, Appl. Catal. A: Gen. 388, 113 (2010). https://doi.org/10.1016/j.apcata.2010.08.043.

[15] Y. Li, Ch.T. Nam, Ch.P. Ooi, J. Phys.: Conf. Ser., 187, 012024 (2009). https://iopscience.iop.org/article/10.1088/1742-6596/187/1/012024.

[16] E. R. Kramer, A.M. Morey, M. Staruch, S.L. Suib, M. Jain, J.I. Budnick, M. Wei, J. Mater. Sci., 48, 665 (2013). https://doi.org/10.1007/s10853-012-6779-2.

[17] A. Zecchina, F. Geobaldo, C. Lamberti, S. Bordiga, G. Turnes Palomino, C. Otero Areán, Catal. Lett., 42, 25 (1996). https://doi.org/10.1007/BF00814463.

[18] M. Mihaylov, E. Ivanova, K. Chakarova, P. Novachka, K. Hadjiivanov, Appl. Catal. A: Gen. 391, 3 (2011). https://doi.org/10.1016/j.apcata.2010.05.014.

[19] R. Ingalls, Phys. Rev., 133, A787 (1964).

https://doi.org/10.1103/PhysRev.133.A787.

[20] G. M. Bancroft, A. G. Maddock, R. G. Burns, Geochimica et Cosmochimica Acta, 31 2219 (1967). https://doi.org/10.1016/0016-7037(67)90062-2.

[21] I. Shinno, L. Zhe, American Mineralogist, 83, 1316 (1998). https://doi.org/10.2138/am-1998-11-1220.

[22] J.Niemantsverdriet, Spectroscopy in Catalysis. An Introduction. 3rd edn (Wiley 2007). https://www.perlego.com/book/2775810/spectroscopy-in-catalysis-pdf.

[23] S.J. Stewart, A.F. Cabrera, N.A. Fellenz, R.C. Mercader, J.F. Bengoa, S.G. Marchetti, J. Phys. Chem. C, 120, 2993 (2016). https://doi.org/10.1021/acs.jpcc.5b10379.

[24] R. Kefirov, E. Ivanova, K. Hadjiivanov, S. Dzwigaj, M. Che, Catal. Lett. 125, 209 (2008). https://doi.org/10.1007/s10562-008-9577-3.

[25] T. Wang, A. Dorner-Reisel, E. Müller, J. Eur. Ceram. Soc., 24, 693 (2004). https://doi.org/10.1016/S0955-2219(03)00248-6.

[26] K. Hadjiivanov, E. Ivanova, R. Kefirov, J. Janas, A. Plesniar, S. Dzwigaj, M. Che, Microporous Mesoporous Mater., 131, 1 (2010). https://doi.org/10.1016/j.micromeso.2009.11.034.

[27] M. Schiavoni, S. Campisi, P. Carniti, A. Gervasini, T. Delplanche, Appl. Catal. A Gen., 563, 43 (2018). https://doi.org/10.1016/j.apcata.2018.06.020.

[28] M. Ferri, S. Campisi, M. Scavini, C. Evangelisti, P. Carniti, A. Gervasini, Appl. Surf. Sci., 475 397 (2019). https://doi.org/10.1016/j.apsusc.2018.12.264.

[29] I. Pérez De Berti, J. Bengoa, N. Fellenz, R. Mercader, S. Marchetti, Rev. Sci. Instrum., 86, 023903 (2015). https://doi.org/10.1063/1.4913382.

[30] Lagarec, K.; Rancourt, D.G. Recoil-Mössbauer Spectral Analysis Software for Windows; University of Ottawa: Ottawa, ON, Canada, (1998).

Figure Captions

Fig. 1: Mössbauer spectra at 298 K after cleaning the sample with He flow.

Fig. 2: Mössbauer spectra at 13 K after cleaning the sample with He flow.

Fig. 3: Mössbauer spectra at 298 K after cleaning the sample with dry medicinal air flow.

Fig. 4: Mössbauer spectra at 13 K after cleaning the sample with dry medicinal air flow.

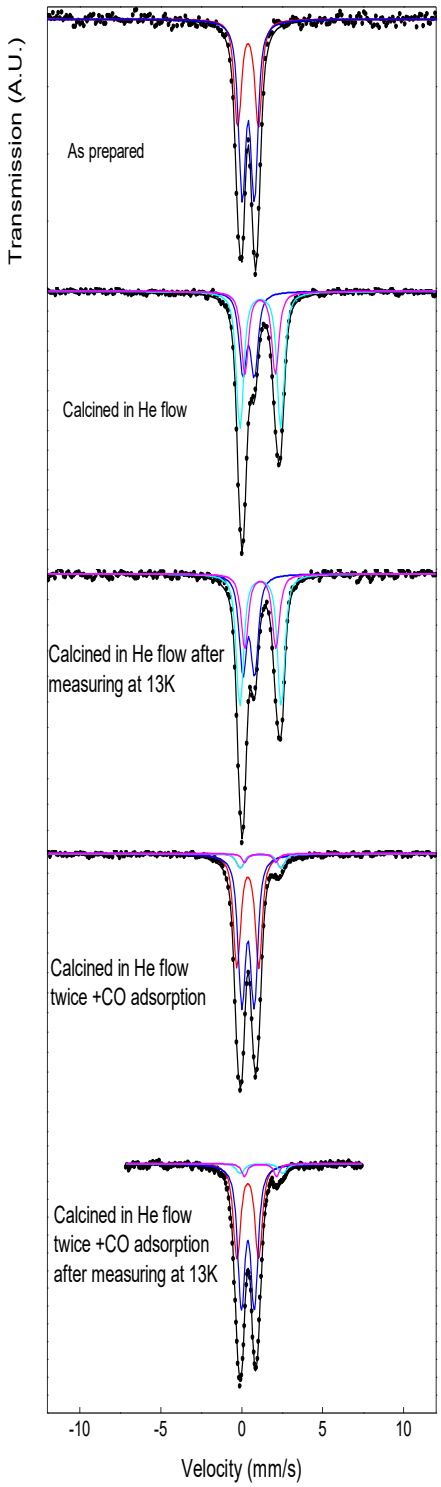
Transmission (A.U.)
As prepared
Calcined in He flow
Calcined in He flow after measuring at 13K
Calcined in He flow twice +CO adsorption
Calcined in He flow twice +CO adsorption after measuring at 13K
-10
-5
0
5
10
Velocity (mm/s)

Figure 1

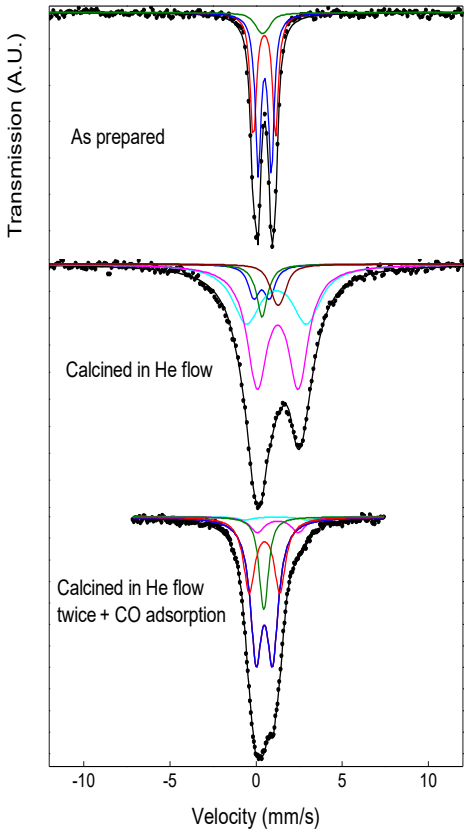
Transmission (A.U.)
As prepared
Calcined in He flow
Calcined in He flow
twice + CO adsorption
-10
-5
0
5
10
Velocity (mm/s)

Figure 2

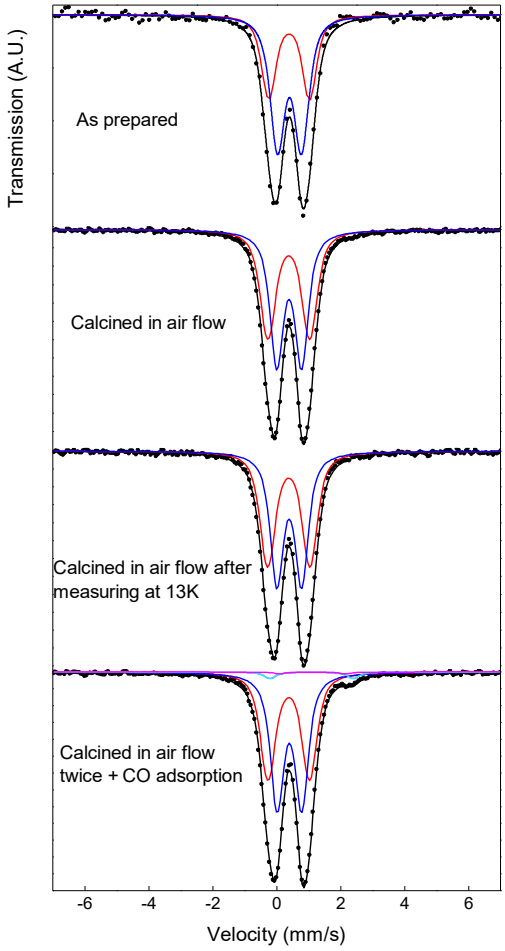
Transmission (A.U.)
As prepared
Calcined in air flow
Calcined in air flow after measuring at 13K
Calcined in air flow twice + CO adsorption
-6
-4
-2
0
2
4
6
Velocity (mm/s)

Figure 3

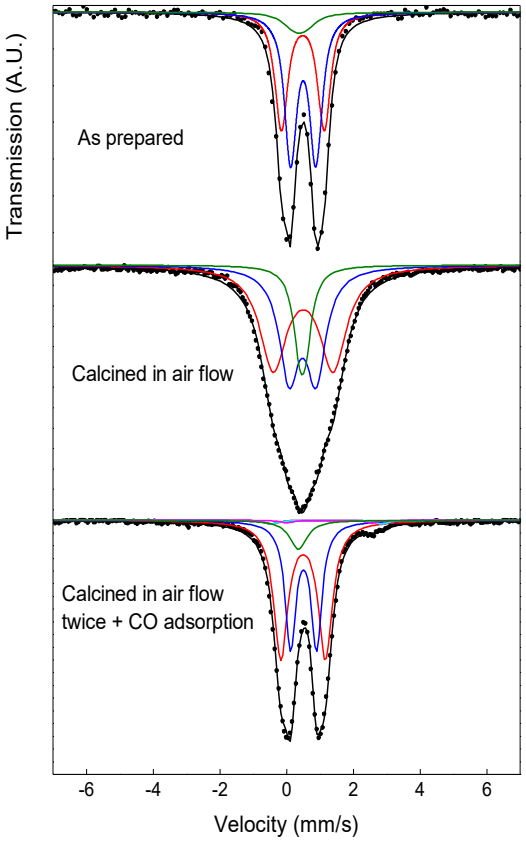
Transmission (A.U.)
As prepared
Calcined in air flow
Calcined in air flow
twice + CO adsorption
-6
-4
-2
0
2
4
6
Velocity (mm/s)

Figure 4

Table 1: Mössbauer parameters of Fe/HAP sample cleaned with He flow and chemisorbed with CO at 298 K.

Code	Parameters			Fe species
	Δ[a] (mm/s)	δ[b] (mm/s)	%[c]	
As prepared	0.76 ± 0.04	0.40 ± 0.01	62 ± 6	Paramagnetic Fe^{3+} replacing Ca(1) ions (blue interaction)
	1.27 ± 0.07	0.39 ± 0.01	38 ± 6	Paramagnetic Fe^{3+} replacing Ca(2) ions (red interaction)
Calcined in He flow	0.72 ± 0.03	0.42 ± 0.02	27 ± 1	Paramagnetic Fe^{3+} replacing Ca(1) ions (blue interaction)
	2.51 ± 0.02	1.15 ± 0.01	46 ± 2	Paramagnetic Fe^{2+} replacing Ca(1) ions (cyan interaction)
	1.89 ± 0.03	1.13 ± 0.01	27 ± 2	Paramagnetic Fe^{2+} replacing Ca(2) ions (magenta interaction)
Calcined in He flow after measuring at 13K	0.73 ± 0.04	0.43 ± 0.02	31 ± 2	Paramagnetic Fe^{3+} replacing Ca(1) ions (blue interaction)
	2.55 ± 0.03	1.16 ± 0.01	44 ± 3	Paramagnetic Fe^{2+} replacing Ca(1) ions (cyan interaction)
	1.93 ± 0.05	1.15 ± 0.02	25 ± 3	Paramagnetic Fe^{2+} replacing Ca(2) ions (magenta interaction)
Calcined in He flow twice + CO adsorption	0.77 ± 0.02	0.39 ± 0.01	53 ± 3	Paramagnetic Fe^{3+} replacing Ca(1) ions (blue interaction)
	1.35 ± 0.03	0.38 ± 0.01	39 ± 3	Paramagnetic Fe^{3+} replacing Ca(2) ions (red interaction)
	2.6 ± 0.2	1.2 ± 0.1	5 ± 1	Paramagnetic Fe^{2+} replacing Ca(1) ions (cyan interaction)
	1.9 ± 0.1	1.13 ± 0.07	3 ± 1	Paramagnetic Fe^{2+} replacing Ca(2) ions (magenta interaction)
Calcined in He flow twice + CO adsorption after measuring at 13K	0.81 ± 0.03	0.38 ± 0.02	55 ± 3	Paramagnetic Fe^{3+} replacing Ca(1) ions (blue interaction)
	1.34 ± 0.03	0.38 ± 0.01	37 ± 3	Paramagnetic Fe^{3+} replacing Ca(2) ions (red interaction)
	2.6 ± 0.6	1.2 ± 0.3	4 ± 1	Paramagnetic Fe^{2+} replacing Ca(1) ions (cyan interaction)
	1.99 ± 0.09	1.16 ± 0.04	4 ± 1	Paramagnetic Fe^{2+} replacing Ca(2) ions (magenta interaction)

[a] quadrupole splitting; [b] isomer shift (all the isomer shifts are referred to α-Fe at 298 K); [c] normalized population of Fe centers.

Table 2: Mössbauer parameters of Fe/HAP sample cleaned with He flow and chemisorbed with CO at 13 K.

Code	Parameters					Fe species
	Δ^a (mm/s)	δ^b (mm/s)	$2\varepsilon^c$ (mm/s)	H^d (kOe)	%^{e}	
As prepared	0.76 ± 0.02	0.50 ± 0.01	-	-	50 ± 2	Paramagnetic Fe^{3+} replacing Ca(1) ions (blue interaction)
	1.28 ± 0.02	0.48 ± 0.01	-	-	42 ± 2	Paramagnetic Fe^{3+} replacing Ca(2) ions (red interaction)
	-	0.38 ± 0.08	0^f	450^f	8 ± 2	$Fe_x(III)O_y$ nanoclusters (2 < size (nm) < 4) (olive interaction)
Calcined in He flow	0.9 ± 0.2	0.3 ± 0.1	-	-	7 ± 2	Paramagnetic Fe^{3+} replacing Ca(1) ions (blue interaction)
	3.5^f	1.19 ± 0.06	-	-	33 ± 3	Paramagnetic Fe^{2+} replacing Ca(1) ions (cyan interaction)
	2.4 ± 0.1	1.26 ± 0.06	-	-	48 ± 3	Paramagnetic Fe^{2+} replacing Ca(2) ions (magenta interaction)
	-	1.3^f	0^f	450^f	6 ± 1	$Fe_x(II)O_y$ nanoclusters (2 < size (nm) < 4) (wine interaction)
	-	0.4 ± 0.1	0^f	450^f	6 ± 2	$Fe_x(III)O_y$ nanoclusters (2 < size (nm) < 4) (olive interaction)
Calcined in He flow twice + CO adsorption	0.96 ± 0.04	0.48 ± 0.01	-	-	50 ± 2	Paramagnetic Fe^{3+} replacing Ca(1) ions (blue interaction)
	1.78 ± 0.05	0.49 ± 0.01	-	-	28 ± 3	Paramagnetic Fe^{3+} replacing Ca(2) ions (red interaction)
	3.6^f	1.2^f	-	-	2 ± 1	Paramagnetic Fe^{2+} replacing Ca(1) ions (cyan interaction)
	2.4^f	1.3^f	-	-	7 ± 1	Paramagnetic Fe^{2+} replacing Ca(2) ions (magenta interaction)
	-	0.45 ± 0.01	0^f	450^f	13 ± 1	$Fe_x(III)O_y$ nanoclusters (2 < size (nm) < 4) (olive interaction)

[a] quadrupole splitting; [b] isomer shift (all the isomer shifts are referred to α-Fe at 298 K); [c] quadrupole shift; [d] hyperfine magnetic field; [e] normalized population of Fe centers; [f] held parameters fixed in fitting.

Table 3: Mössbauer parameters of Fe/HAP sample cleaned with dry medicinal air flow and chemisorbed with CO at 298 K.

Code	Parameters			Fe species
	Δ[a] (mm/s)	δ[b] (mm/s)	%[c]	
As prepared	0.76 ± 0.04	0.40 ± 0.01	62 ± 6	Paramagnetic Fe^{3+} replacing Ca(1) ions (blue interaction)
	1.27 ± 0.07	0.39 ± 0.01	38 ± 6	Paramagnetic Fe^{3+} replacing Ca(2) ions (red interaction)
Calcined in air flow	0.78 ± 0.01	0.39 ± 0.01	48 ± 1	Paramagnetic Fe^{3+} replacing Ca(1) ions (blue interaction)
	1.31 ± 0.02	0.38 ± 0.01	52 ± 1	Paramagnetic Fe^{3+} replacing Ca(2) ions (red interaction)
Calcined in air flow after measuring at 13K	0.78 ± 0.01	0.39 ± 0.01	49 ± 2	Paramagnetic Fe^{3+} replacing Ca(1) ions (blue interaction)
	1.32 ± 0.02	0.38 ± 0.01	51 ± 2	Paramagnetic Fe^{3+} replacing Ca(2) ions (red interaction)
Calcined in air flow after twice + CO adsorption	0.77 ± 0.01	0.40 ± 0.01	52 ± 2	Paramagnetic Fe^{3+} replacing Ca(1) ions (blue interaction)
	1.30 ± 0.02	0.38 ± 0.01	45 ± 2	Paramagnetic Fe^{3+} replacing Ca(2) ions (red interaction)
	2.6 ± 0.2	1.09 ± 0.09	2 ± 1	Paramagnetic Fe^{2+} replacing Ca(2) ions (cyan interaction)
	2.1[f]	1.1[f]	1 ± 1	Paramagnetic Fe^{2+} replacing Ca(1) ions (magenta interaction)

[a] quadrupole splitting; [b] isomer shift (all the isomer shifts are referred to α-Fe at 298 K); [c] normalized population of Fe centers.

Table 4: Mössbauer parameters of Fe/HAP sample cleaned with dry medicinal air flow and chemisorbed with CO at 13 K.

Code	Parameters					Fe species
	Δ[a] (mm/s)	δ[b] (mm/s)	2ε[c] (mm/s)	H[d] (kOe)	%[e]	
As prepared	0.76 ± 0.02	0.50 ± 0.01	-	-	50 ± 2	Paramagnetic Fe^{3+} replacing Ca(1) ions (blue interaction)
	1.28 ± 0.02	0.48 ± 0.01	-	-	42 ± 2	Paramagnetic Fe^{3+} replacing Ca(2) ions (red interaction)
	-	0.38 ± 0.08	0[f]	450[f]	8 ± 2	$Fe_x(III)O_y$ nanoclusters (2 < size (nm) < 4) (olive interaction)
Calcined in air flow	0.80 ± 0.02	0.50 ± 0.01	-	-	38 ± 1	Paramagnetic Fe^{3+} replacing Ca(1) ions (blue interaction)
	1.80 ± 0.02	0.48 ± 0.01	-	-	48 ± 1	Paramagnetic Fe^{3+} replacing Ca(2) ions (red interaction)
	-	0.48 ± 0.01	0[f]	450[f]	14 ± 2	$Fe_x(III)O_y$ nanoclusters (2 < size (nm) < 4) (olive interaction)
Calcined in air flow twice + CO adsorption	0.78 ± 0.01	0.50 ± 0.01	-	-	37 ± 1	Paramagnetic Fe^{3+} replacing Ca(1) ions (blue interaction)
	1.33 ± 0.01	0.50 ± 0.01	-	-	53 ± 1	Paramagnetic Fe^{3+} replacing Ca(2) ions (red interaction)
	3.3[f]	1.2[f]	-	-	2 ± 1	Paramagnetic Fe^{2+} replacing Ca(2) ions (cyan interaction)
	2.6[f]	1.3[f]	-	-	1 ± 1	Paramagnetic Fe^{2+} replacing Ca(1) ions (magenta interaction)
	-	0.35 ± 0.02	0[f]	450[f]	7 ± 1	$Fe_x(III)O_y$ nanoclusters (2 < size (nm) < 4) (olive interaction)

[a] quadrupole splitting; [b] isomer shift (all the isomer shifts are referred to α-Fe at 298 K); [c] quadrupole shift; [d] hyperfine magnetic field; [e] normalized population of Fe centers; [f] held parameters fixed in fitting.